Available online at www.sciencedirect.com
SCIENCE DIRECT®
Engineering Fracture Mechanics 72 (2005) 2584–2601
Engineering Fracture Mechanics
www.elsevier.com/locate/engfracmech

Initiation and arrest of an interfacial crack in a four-point bend test

Zhenyu Huang [a], Z. Suo [a,*], Guanghai Xu [b], Jun He [b], J.H. Prévost [c], N. Sukumar [d]

[a] Division of Engineering and Applied Sciences, Harvard University, Cambridge, MA 02138, USA
[b] Intel Corporation, 2501 NW 229th Avenue, Hillsboro, OR 97124, USA
[c] Civil and Environmental Engineering Department, Princeton University, Princeton, NJ 08544, USA
[d] Civil and Environmental Engineering Department, University of California, Davis, CA 95616, USA

Received 24 February 2005; received in revised form 13 April 2005; accepted 23 April 2005
Available online 29 June 2005

Abstract

This paper describes a framework to study the initiation and arrest of an interfacial crack, using a combination of experiment and computation. We consider a test configuration widely used in the microelectronic industry: a sample of two substrates bonded by a stack of thin films, with a pre-crack in one of the substrates, perpendicularly impinging upon the films. When the sample is loaded to a critical level, the pre-crack initiates a new crack on one of the interfaces in the sample. The new crack often runs rapidly on the interface for a considerable length, and then arrests. We introduce a quantity, the *initiation energy*, to characterize the condition under which the pre-crack initiates the interfacial crack. The initiation energy is independent of the test configuration on the scale of the substrates, but changes greatly with the materials and stacking sequence of the films. We measure the initiation energy experimentally, interpret the data using mechanistic models, and use the initiation energy to predict the arrest crack length.

Keywords: Thin film; Interfacial fracture; Crack initiation; Crack arrest; Four-point bend

1. Introduction

Modern devices are structures of complex architectures, diverse materials, and small features [1,2]. In such devices, many processes (e.g., material deposition, temperature change and electromigration) induce

* Corresponding author. Tel.: +1 617 4953789; fax: +1 617 4960601.
E-mail address: suo@deas.harvard.edu (Z. Suo).

0013-7944/$ - see front matter © 2005 Elsevier Ltd. All rights reserved.
doi:10.1016/j.engfracmech.2005.04.002

stresses [3,4]. The stresses may cause dissimilar materials to separate, which is a main failure mode of the devices. The adhesion between two materials is characterized by the *extension energy* of an interfacial crack, Γ [5,6]. No reliable method exists to calculate Γ from first principles; rather, Γ is measured experimentally. In the microelectronic industry, the measurements of the crack extension energy have become an integral part in developing materials, architectures and processes [7–9].

As a pre-requisite to measuring the crack extension energy of an interface, a sharp crack must be introduced on the interface. A common procedure is to first introduce in a sample a pre-crack that impinges upon the interface. When the sample is loaded to a critical level, the pre-crack initiates a new crack on the interface. The new crack often runs rapidly on the interface for a considerable length, and then arrests. The subsequent load that stably extends the interfacial crack gives a reading of Γ. Consequently, to obtain a reading, it is crucial that the interfacial crack arrests within a reasonable length.

The arrest crack length depends on both the initiation and the extension of the interfacial crack. While crack extension has been well studied, its initiation has received less attention [10]. We experimentally measure the critical load for the pre-crack to initiate the interfacial crack, and then convert the critical load to a quantity Λ, which we call the *initiation energy*. The initiation energy varies greatly with the bonding materials and processes, but is independent of the test configuration at the scale of the substrates. Once obtained, the initiation energy can be used to predict the critical load for a pre-crack to initiate an interfacial crack in any other test configuration, so long as the bonding materials and processes are the same. Furthermore, the initiation energy can be used to predict the arrest crack length.

We illustrate these ideas using samples comprising two silicon substrates bonded by a stack of thin films, subject to four-point bend. Section 2 summarizes the salient features of the four-point bend test. Section 3 defines the initiation energy, and reports its experimental values. Section 4 calculates the arrest crack length. Section 5 describes mechanistic models of the initiation energy. Section 6 discusses assumptions made in the earlier sections, and provides perspectives for future research.

2. The four-point bend test

A large number of methods exist to measure the interfacial crack extension energy Γ; see reviews [11–13]. The four-point bend test is a method of choice in several industrial and academic laboratories [6,8,9,14–16]. Fig. 1 sketches a test system, and Fig. 2 sketches a sample. The procedure is as follows. Deposit a stack of thin films of concern on one silicon substrate. Use a thin layer of epoxy to glue a second silicon substrate to the film on the top. The entire film stack is much thinner than the either substrate. Use a diamond blade to make a notch in one of the substrates. Place the sample between four load pins. Program an actuator to ramp up the displacement Δ, and read the force P from a load cell.

Fig. 3 is a schematic of the force–displacement diagram. After securing various contacts, the force rises linearly with the actuation displacement. At a certain force, indicated in the diagram by a square, a crack emanates from the notch root, and stops somewhere in the film stack. This crack is called the *pre-crack*. The precise location of the pre-crack front is specific to the film stack, and is not controlled in the experiment. The pre-crack remains dormant for some time as the actuator ramps up the displacement further. At a critical force, P_c, an *interfacial crack* initiates on one of the interfaces. The interfacial crack runs rapidly, and arrests at a length a_{arrest} (typically several times the substrate thickness). So short is the time between the initiation and the arrest of the interfacial crack that, during the process, the actuation displacement remains nearly unchanged. Denote this critical displacement by Δ_c. The formation of the large interfacial crack increases structural compliance, so that the force drops. After the instability, the displacement ramps up further, and the interfacial crack extends stably at a plateau force, P_{plateau}.

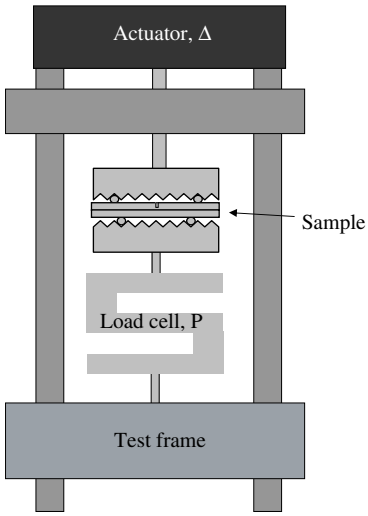

Fig. 1. A schematic of the four-point bend test system. Place the sample between the four load pins. Program the actuator to ramp up the displacement Δ. The load cell reads the force P.

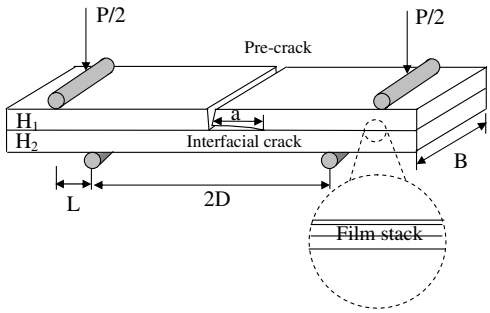

Fig. 2. A schematic of a sample. Representative dimensions: width of the substrates $B = 7.8$ mm, thickness of the substrates $H_1 = H_2 = 0.75$ mm, distance between the inner and outer pins $L = 4$ mm, and distance between the inner pins, $2D = 27$ mm. The thickness of the film stack is on the order of microns.

The energy release rate of the interfacial crack, G, takes the form

$$G = g\frac{L^2P^2}{\overline{E}B^2H^3}. \tag{1}$$

With reference to Fig. 2, L is the distance between an inner and an outer load pin (i.e., the moment arm), and $2D$ is the distance between the two inner load pins. The two substrates have thicknesses H_1 and H_2 width B, Young's modulus E, and Poisson's ratio v; $H = (H_1 + H_2)/2$, and $\overline{E} = E/(1 - v^2)$. In general, the normalized energy release rate, g, depends on the interfacial crack length a, and on the film stack (i.e., on the thicknesses and deformation behavior of constituent materials). However, when the interfacial crack length a is long compared to film stack thickness, g becomes independent of the film stack. Furthermore, when the interfacial crack length a is long compared to the substrate thickness, g becomes independent of a, and asymptotes to a plateau [14]:

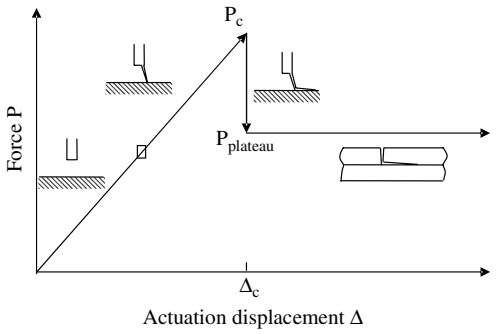

Fig. 3. A schematic of the force–displacement diagram. The actuator is programmed to ramp up the displacement. Initially, the force increases linearly with the displacement. At a certain force, marked by a square in the diagram, a pre-crack emanates from the notch root and stops at the interface. The displacement ramps up further. At a critical force P_c, the pre-crack initiates an interfacial crack. The new crack runs rapidly on an interface in the film stack, and then arrests. During the process, the displacement remains at Δ_c, and the force drops. As the displacement ramps up further, the interfacial crack extends stably, and the force attains a plateau P_{plateau}.

$$g_{\text{plateau}} = \frac{3\eta(3 - 3\eta + \eta^2)}{16(1-\eta)^3}, \tag{2}$$

where $\eta = H_1/(H_1 + H_2)$ is the substrate thickness ratio. The interfacial crack extends when $G = \Gamma$. Eq. (1) at the plateau converts the measured P_{plateau} to the crack extension energy Γ. (To focus on the main ideas with minimal complication in this paper, we assume a constant Γ, except for a discussion in Section 6.)

The four-point bend test can measure the interfacial crack extension energy for very thin films, fabricated by the same processes as actual devices. Although both the pre-crack and the interfacial crack are introduced by unstable processes, it is the plateau force that gives the reading of Γ. The conversion from the plateau force to the interfacial crack extension energy requires no information about the film stack. Nor is any measurement of the crack length necessary.

Fig. 4 illustrates one film stack used in our experiments. The carbon-doped oxide (CDO), also known as the organosilicate glass, is a low-permittivity dielectric. The silicon nitride (SiN_xH_y) is an etch stop. We are concerned with the adhesion between these two materials, which are representative in the new generation of on-chip interconnect structures. We thermally oxidize two silicon substrates. On substrate 1 is deposited a film of CDO, followed by a film of SiN_xH_y. A layer of epoxy glues substrate 2 to substrate 1. Substrate 1 is pre-cracked. The actuator ramps up the displacement at a rate of 2 μm/s prior to the critical force, and at a rate of 0.02 μm/s in the plateau region. The new crack runs on the CDO/SiN_xH_y interface. Of ten samples tested, sample A7 breaks substrate 2, and samples A8, A9 and A10 exhibit no plateaus. The six other samples (A1–A6) exhibit plateaus. In our experiments, the two substrates have the same thickness, so that $g_{\text{plateau}} = 21/16$. Using Eq. (1), we convert the measured plateau force of each sample to a value of the interfacial crack extension energy, as listed in Table 1. The interfacial crack extension energy has a mean $\Gamma = 4.2$ J/m^2 and a small scatter.

Quite often, after initiation the interfacial crack arrests only on arrival at the inner load pin. When this happens, the force–displacement diagram exhibits no plateau, and no reliable information is obtained on the interfacial crack extension energy. Samples A8, A9 and A10 behave this way. To show this behavior more clearly, we test samples with a different film stack (Fig. 5). On substrate 1 is deposited a film of SiN_xH_y, followed by a film of CDO. Substrate 2 is then glued to the face of the CDO. Notch substrate 2, and the pre-crack must rupture the epoxy layer before initiating a crack on the SiN_xH_y/CDO interface. Because a large force is needed for the epoxy layer to rupture, the sample is overloaded when the interfacial crack initiates. After initiation, the new crack runs on the CDO/SiN_xH_y interface, and arrests at the inner load pin. The force–displacement diagram exhibits no plateau, giving no reading of the extension energy.

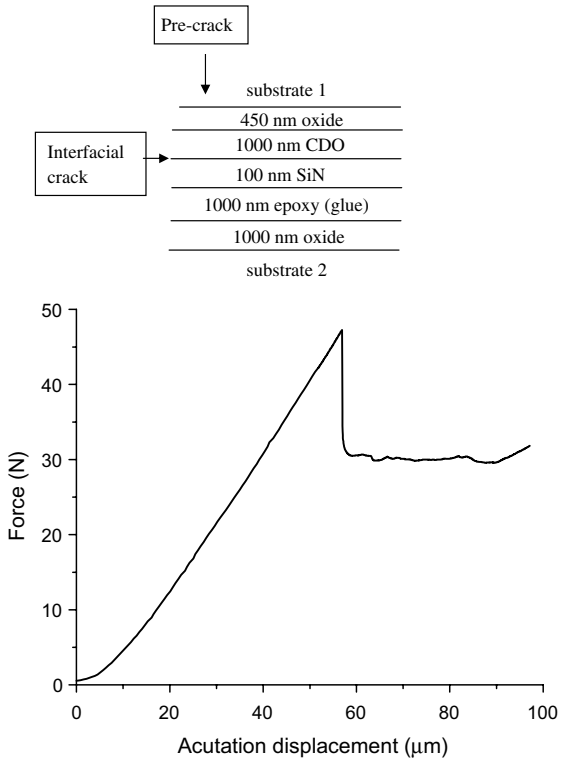

Fig. 4. A film stack used in experiments, and an experimental record of the force–displacement diagram.

Table 1
Experimental values of the crack extension energy Γ and the crack initiation energy Λ

	Sample					
	A1	A2	A3	A4	A5	A6
Γ (J/m^2)	4.24	4.26	4.39	4.00	3.91	4.41
Λ (J/m^2)	26.4	28.1	30.9	22.3	29.5	32.9
Λ/Γ	7.12	7.19	7.77	6.19	8.25	8.39

The film stack is shown in Fig. 4.

3. Initiating an interfacial crack

Crack deflection at an interface has been studied for some time, mainly motivated by the development of all-ceramic composites for high temperature applications [17]. Such a composite embeds ceramic fibers in a ceramic matrix. For the composite to be ductile, a crack in the matrix must deflect at the interfaces between the fibers and the matrix, rather than penetrates the fibers. A main mechanics result is the ratio of the energy release rate of a deflection crack to that of a penetration crack (e.g. [18]). This ratio is compared with the ratio of the crack extension energy of the fiber/matrix interface to that of the fiber.

In this paper, we assume that deflection wins the competition: the pre-crack in the substrate will deflect onto an interface in the film stack. We study the arrest of the interfacial crack after a substantial extension.

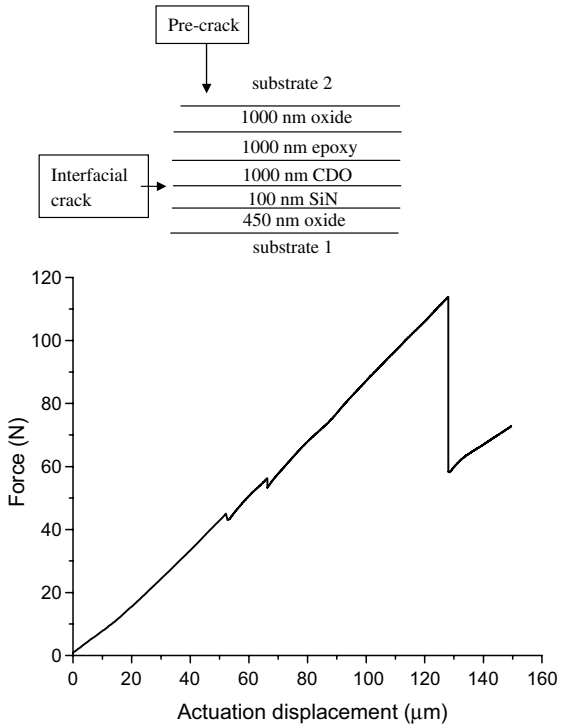

Fig. 5. A second film stack used in experiments. The pre-crack ruptures the epoxy layer first, and then initiates a crack on the CDO/SiN interface. After initiation, the interfacial crack runs rapidly to the inner load pin. No plateau is recorded.

The winner declared, the *ratio* of the deflection to penetration energy release rate no longer concerns us. Instead, we need to know the *magnitude* of the force that initiates the interfacial crack.

Given the multiple materials and inelastic deformation in the film stack, it is unlikely that any microscopic model can predict accurately the critical force for the pre-crack to initiate the interfacial crack. We pursue a pragmatic approach in this section, and leave the microscopic models to a later section. The critical force for initiation, P_c, is readily measured. We convert the critical force to the initiation energy. The situation is analogous to converting the load to extend a crack to the crack extension energy. The former depends on specimen geometry, but the latter does not. We next introduce the crack initiation energy in the same way as the crack extension energy.

For the pre-crack impinging upon the film stack, the stress field in the film stack is complicated, depending on the materials and stacking sequence, the precise location of the crack front, and the inelastic deformation in the films. However, in the substrates, at some distance away from the film stack, the stress field is the same as that of a crack in a homogeneous elastic material. The film stack is much thinner than the substrates. Consequently, an annulus exists, its inner radius being some multiple of the thickness of the film stack, and its outer radius being some fraction of the thickness of the substrates (Fig. 6). Inside the annulus, the stress field (i.e., the classical square-root singularity) depends on the external load and sample geometry through a single parameter: the energy release rate of the pre-crack, G_{pre}. That is, G_{pre} is the only messenger between the macroscopic boundary conditions and the microscopic processes at the crack front.

The energy release rate G_{pre} of the pre-crack increases with the force P. At the critical force P_c, the pre-crack initiates an interfacial crack. We define the initiation energy, Λ, as the energy release rate G_{pre} of the pre-crack at this critical force. Analogous to the fracture energy of a material, the initiation energy Λ is

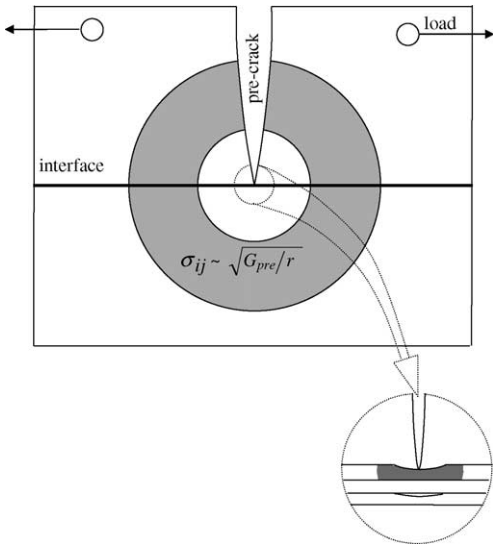

Fig. 6. The film stack is much thinner than the substrates. The inner radius of the annulus is some multiple of the film thickness, and the outer radius some fraction of the substrate thickness. The stress field in the annulus is the universal square-root singularity that prevails around a crack in a homogeneous elastic solid. At a length comparable to the film thickness, the stress field depends on details of the film stack (i.e., on inelastic deformation and flaws). At a length comparable to the substrate thickness, the stress field depends on details of the test configuration (i.e., on the sample geometry and the load distribution).

independent of the test configuration on the scale of the substrates (e.g., independent of the thicknesses of the substrates and the positions of the load pins). However, Λ is specific to the materials of the films, their stacking sequence, and the flaws in the stack.

For the four-point bend specimen, the energy release rate of the pre-crack, G_{pre}, takes the form of Eq. (1), but with its own dimensionless coefficient [19]:

$$g_{\text{pre}} = 1.917 \sin\left(\frac{\pi\eta}{2}\right)\left(1 + 0.216\left[1 - \sin\left(\frac{\pi\eta}{2}\right)\right]^4\right)^2\left[\cos\left(\frac{\pi\eta}{2}\right)\right]^{-3}. \tag{3}$$

The experimental value of the critical force for initiation, P_c, is converted to the initiation energy Λ according to Eqs. (1) and (3).

When the two substrates have the same thickness, $g_{\text{pre}} = 3.846$. Table 1 lists the values of the initiation energy for the film stack shown in Fig. 4. The initiation energy has a mean $\Lambda = 28.4$ J/m^2, with a scatter larger than that of the crack extension energy Γ. For the other film stack (Fig. 5), where the pre-crack has to rupture the epoxy layer before the interfacial crack initiates, Table 2 lists the experimental values of the initiation energy of nine samples tested. The initiation energy has a mean $\Lambda = 112$ J/m^2, with a large scatter.

The crack extension energy in silicon is about 6 J/m^2. The energy needed to initiate a crack from the notch root is higher than that, but is much below the interfacial crack initiation energy measured in our

Table 2
Experimental values of the crack initiation energy for the film stack shown in Fig. 5

	Sample								
	B1	B2	B3	B4	B5	B6	B7	B8	B9
Λ (J/m^2)	97	224	171	96	40	94	72	150	60

experiments. The difference accounts for the experimental observation that the force for the notch to initiate the pre-crack is much below the force for the pre-crack to initiate the interfacial crack.

4. Arresting an interfacial crack

As illustrated in Fig. 1, the actuator is programmed to ramp up the displacement Δ. The sample and the test machine are taken to be linearly elastic, loaded in series. The actuation displacement Δ is the sum of the displacement of the test machine and that between the upper and lower load pins. For a fixed interfacial crack length a, the actuation displacement is linear in the force, $\Delta = CP$. The compliance, C, includes both the compliance of the test machine, C_M, and that of the sample. The compliance of the sample increases with the crack length a. On the displacement–force diagram, the slope of the line connecting a given point (Δ, P) to the origin gives the compliance. For the four-point bend specimen, the force–displacement relation takes the form

$$\Delta = c\frac{L^2 P}{\bar{E}BH^2}, \tag{4}$$

where c is the normalized compliance.

A combination of Eqs. (1) and (4) gives the energy release rate as a function of the actuation displacement:

$$G = \left(\frac{g}{c^2}\right)\left(\frac{\bar{E}H}{L^2}\right)\Delta^2. \tag{5}$$

This form of energy release rate is applicable to both the pre-crack and the interfacial crack. For the pre-crack, the dimensionless coefficient is g_{pre}/c_0^2, where c_0 is the normalized compliance before the interfacial crack initiates. For the interfacial crack, the dimensionless coefficient is $g(a)/[c(a)]^2$, which is a function of the interfacial crack length a.

The energy release rate of the pre-crack is a function of the actuation displacement, $G_{pre}(\Delta)$. At a critical displacement, Δ_c, the energy release rate reaches the initiation energy, $G_{pre}(\Delta_c) = \Lambda$.

The energy release rate of the interfacial crack, G, is a function of the actuation displacement Δ and the interfacial crack length a. When the system is overloaded, $G(\Delta, a) > \Gamma$, the interfacial crack grows. When the system is underloaded, $G(\Delta, a) < \Gamma$, the interfacial crack stops. Many causes exist for overload. For example, the pre-crack may need to rupture a tough film before the interfacial crack initiates (Fig. 5). Right after the tough film ruptures, the force is higher than that needed for the crack to extend on the interface. Fig. 7 sketches another cause of overload. The energy release rate of the interfacial crack, G, is shown as a function of the crack length at several fixed level of the displacement Δ. Let a_{flaw} be the initial length of a flaw on the interface from which the interfacial crack will initiate. When the displacement is small, $\Delta < \Delta_c$, the energy release rate is below the crack extension energy, $G(a_{flaw}, \Delta) < \Gamma$, so that the flaw remains dormant. At the critical displacement Δ_c, $G(a_{flaw}, \Delta_c) = \Gamma$ and the interfacial crack starts to grow. The energy release rate then exceeds the crack extension energy.

An overloaded interfacial crack runs faster than the actuator can respond; between the crack initiation and arrest, the actuation displacement remains unchanged from Δ_c. Whatever the cause of overload, the crack will arrest if the energy release rate decreases sufficiently to satisfy $G(\Delta_c, a_{arrest}) = \Gamma$.

Taking the ratio of the initiation condition, $G_{pre}(\Delta_c) = \Lambda$, and the arrest condition, $G(\Delta_c, a_{arrest}) = \Gamma$, we obtain that

$$\left[\frac{g_{pre}}{g(a_{arrest})}\right]\left[\frac{c(a_{arrest})}{c_0}\right]^2 = \frac{\Lambda}{\Gamma}. \tag{6}$$

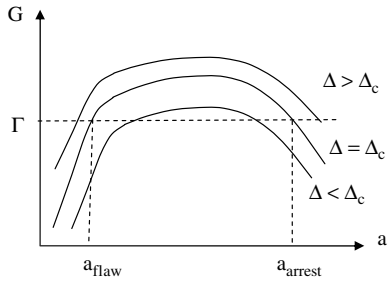

Fig. 7. Schematic of the energy release rate G as a function of the crack length a at several constant level of the displacement Δ. The crack extension energy Γ is taken to be a constant, and the crack extends if $G > \Gamma$. At the critical displacement Δ_c, the crack initiates at the flaw size a_{flaw}, runs unstably, and arrests at the length a_{arrest}. As the displacement ramps up further, the crack extends stably.

This nonlinear equation determines the arrest crack length, a_{arrest}. This result is applicable to all test configurations, so long as we use a consistent normalization. The initiation-to-extension energy ratio, Λ/Γ, measures the degree of overload. The higher the initiation energy, the larger the crack arrest length. The normalized compliance $c(a)$ always increases with the crack length. The normalized energy release rate $g(a)$ may be a complex function of the crack length, depending on the specimen geometry. The arrest crack length is short if $c(a)$ is a sharp increasing function, or $g(a)$ is a sharp decreasing function.

Eqs. (3) and (2) give the normalized energy release rate for the pre-crack and for the interfacial crack. We need to obtain the normalized compliances. Denote the length of a generic crack by b. The elastic energy stored in the sample and the machine is a function of the displacement and the crack length, $U(\Delta, b) = \Delta^2/2C$. By definition, the energy release rate is the reduction of the elastic energy associated with the unit area of crack advance, when the external load is rigidly held and does no work; that is, $G = -\partial U(\Delta, b)/B\partial b$. Consequently, the two functions, $g(b)$ and $c(b)$, are connected by $dc/db = 2g/H$ (see [19]). We can obtain the normalized compliance by integrating the normalized energy release rate.

We now apply the general theory to the four-point bend test. Before the interfacial crack initiates, the initial compliance of the system, c_0, has three contributions:

$$c_0 = \frac{C_M \overline{E} B H^2}{L^2} + \frac{3D + L}{4H} + c_{pre}. \tag{7}$$

The first contribution comes from the machine compliance C_M, which can be determined experimentally. The second contribution comes from the bending of an unnotched sample obtained by beam theory. The third contribution comes from the introduction of the pre-crack into the perfect beam, given by [19]

$$c_{pre} = \left(\frac{\eta}{1-\eta}\right)^2 \left(8.895 - 29.535\eta + 55.71\eta^2 - 53.76\eta^3 + 19.68\eta^4\right). \tag{8}$$

When the pre-cracked substrate is much thinner than the other substrate, the compliance of the perfect beam prevails over that due to the pre-crack. The situation is reversed when the pre-cracked substrate is thicker than the other substrate.

After the interfacial crack initiates, the system gains additional compliance, which can be calculated by integrating the energy release rate of the interfacial crack. For a long interfacial crack, $a > H$, the normalized energy release rate reaches the plateau $g_{plateau}$, Eq. (2). Consequently, in the presence of a long interfacial crack, the normalized compliance of the system is

$$c(a) = 2g_{plateau} a/H + c_0. \tag{9}$$

Inserting the expressions for the normalized energy release rates and compliances into Eq. (6), we obtain the arrest crack length in the four-point bend test:

$$a_{\text{arrest}} = \frac{(0.75D + 0.25L) + (c_{\text{pre}} + C_{\text{M}}\bar{E}BH^2/L^2)H}{2\sqrt{g_{\text{plateau}}g_{\text{pre}}}}\left(\sqrt{\frac{\Lambda}{\Gamma}} - \sqrt{\frac{g_{\text{pre}}}{g_{\text{plateau}}}}\right). \tag{10}$$

Both g_{pre} and g_{plateau} increases with the thickness ratio $H_1/(H_1 + H_2)$. The ratio $g_{\text{pre}}/g_{\text{plateau}}$ ranges from 7.902 when the pre-cracked substrate is very thin, to 2.634 when the pre-cracked substrate is very thick (Fig. 8). When $\Lambda/\Gamma > g_{\text{pre}}/g_{\text{plateau}}$, the interfacial crack is overloaded and is unstable after initiation. When $\Lambda/\Gamma < g_{\text{pre}}/g_{\text{plateau}}$, the interfacial crack is stable after initiation.

Fig. 9 plots the arrest crack length as a function of the substrate thickness ratio, at several levels of the initiation-to-extension energy ratio Λ/Γ, assuming the machine compliance is negligible. The arrest crack

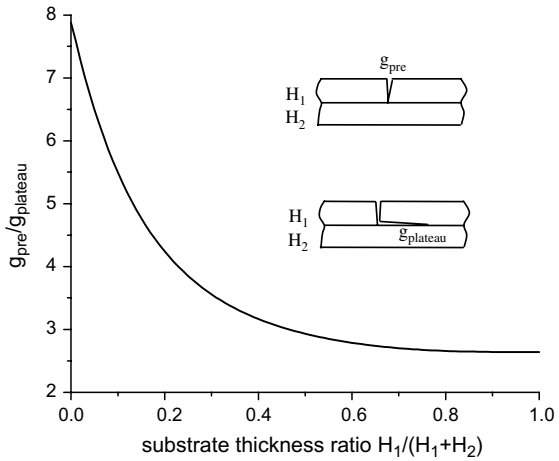

Fig. 8. The ratio $g_{\text{pre}}/g_{\text{plateau}}$ as a function of the substrate thickness ratio.

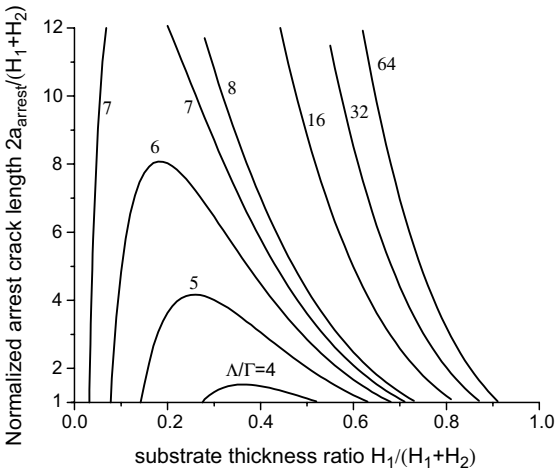

Fig. 9. The arrest crack length as a function of the substrate thickness ratio, at several values of the initiation-to-extension energy ratio Λ/Γ. The substrate of thickness H_1 is notched. The machine compliance is taken to be negligible compared to the sample. $(3D + L)/(H_1 + H_2) = 29.66$.

length decreases as the pre-cracked substrate becomes thicker than the other substrate. If the machine compliance is significant compared to the sample compliance, the arrest crack length is larger than that given in Fig. 9, and should be calculated from Eq. (10).

When the two substrates have an equal thickness, $H_1 = H_2 = H$, $c_{\text{pre}} = 2.53$, $g_{\text{plateau}} = 21/16$ and $g_{\text{pre}} = 3.864$. Specializing Eq. (10), we obtain the arrest crack length

$$a_{\text{arrest}} = \left[0.0555(3D + L) + \left(0.562 + 0.223 C_{\text{M}} \overline{E} B H^2/L^2\right) H\right]\left(\sqrt{\Lambda/\Gamma} - 1.716\right). \tag{11}$$

In our experiments, the sample dimensions are $D = 13.5$ mm, $L = 4$ mm, $H = 0.75$ mm. $(3D + L)/4H = 14.83$, and $C_{\text{M}}\overline{E}BH^2/L^2 = 36$. For the film stack illustrated in Fig. 4, the measured initiation-to-extension energy ratio is about $\Lambda/\Gamma = 8$. Eq. (11) predicts the arrest crack length in the range $a_{\text{arrest}} = 10.7$ mm. Our experimental observations fall in this range.

For the film stack illustrated in Fig. 5, the mean initiation energy is $\Lambda = 112$ J/m^2. Because the crack extends on the CDO/SiN interface, we assume that the same crack extension energy applies, $\Gamma = 4.2$ J/m^2, which gives $\Lambda/\Gamma \approx 27$. Eq. (11) gives $a_{\text{arrest}} = 14$ mm even for a small machine compliance $C_{\text{M}}\overline{E}BH^2/L^2 = 7$. Indeed, in this case, the interfacial crack arrests at the inner load pin. The force–displacement diagram exhibits no plateau.

For the case that the two substrates have an equal thickness, $H_1 = H_2 = H$, we have obtained the energy release rate as a function of the interfacial crack length. The arrest crack length is much larger than the film thickness, so that the effect of the films on the energy release rate is negligible. When the interfacial crack length is comparable or larger than the substrate thickness, g is independent of the crack length, $g = 21/16$. When the crack is short compared to the substrate thickness, the energy release rate of the interfacial crack relates to that of the pre-crack as $g = 0.26 g_{\text{pre}}$ [18]. Recall that $g_{\text{pre}} = 3.846$. Combining the two results, we obtain the limit $g \to 1.00$ as $a/H \to 0$. We have calculated the energy release rate for intermediate crack length using a finite element method (Appendix A). The finite element results, together with the two limits, suggest the following fit:

$$g(a) = 1.313 - 0.313 \exp(-5.74 a/H). \tag{12}$$

The normalized energy release rate increases with the crack length, and is nearly at the plateau when the crack length is about the substrate thickness. We obtain the compliance by integrating the energy release rate, giving

$$c(a) = c_0 + 2.626 \frac{a}{H} + 0.114\left[\exp\left(-5.74 \frac{a}{H}\right) - 1\right]. \tag{13}$$

Fig. 10 plots the energy release rate as a function of the crack length, holding the actuation displacement constant. The trend of the curve is readily understood. When the crack length a goes beyond the substrate thickness H, the compliance increases with the crack length, but g reaches the plateau value, so that G decreases as the crack length increases. In the other limit, when $a \ll H$, the compliance is insensitive to the small crack length, but g increases with the crack length, so that G increases with the crack length. As pointed out before, this functional shape leads to overload after the interfacial crack initiates. Because the machine compliance is independent of the crack length, a large machine compliance makes the energy release rate flatter at the long crack length, increasing the arrest crack length.

In deriving Eq. (11), we have assumed that the arrest crack is long compared to the substrate thickness, so that the normalized energy release rate of the interfacial crack, g, has reached the plateau, and the compliance is linear in the crack length. To ascertain the accuracy of this approximation, we insert the full expressions of $g(a)$ and $c(a)$ into Eq. (6). Fig. 11 plots the arrest crack length as a function of the energy ratio Λ/Γ and the machine compliance. The plateau approximation, Eq. (11), is also plotted for comparison. The approximation is excellent, except for very small arrest crack length.

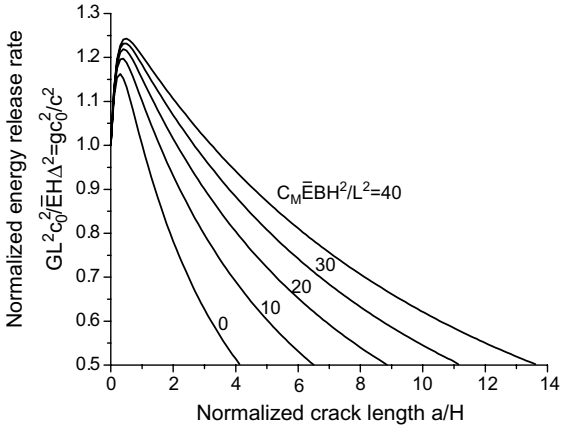

Fig. 10. The energy release rate of the interfacial crack as a function of the crack length, while the actuation displacement is held constant. The two substrates have the same thickness, H, and $(3D + L)/H = 59.32$.

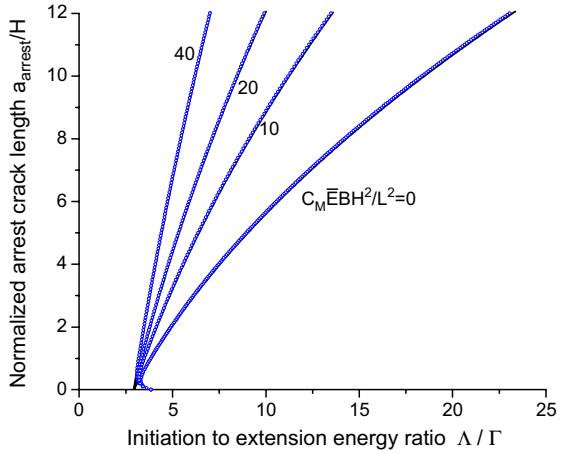

Fig. 11. The arrest crack length as a function of the initiation-to-extension energy ratio Λ/Γ and the machine compliance. The two substrates have the same thickness, H, and $(3D + L)/H = 59.32$.

5. Mechanistic models of the initiation energy

The initiation energy can be measured experimentally, regardless the nature of the film stack or the microscopic process that leads to the initiation of the interfacial crack. Nonetheless, microscopic models shed light on the initiation energy measured experimentally. This section describes several such models.

We first establish a lower bound to the initiation energy. Consider the scenario that the pre-crack readily penetrates the films prior to the interface on which an interfacial crack will initiate. When the front of the pre-crack arrives at the interface, the load is still so low that flaws on the interface are dormant. As the load ramps up and reaches a critical level, the energy release rate G of an interfacial flaw reaches Γ, and the flaw initiates an interfacial crack. If the pre-existing flaw size exceeds some multiple of the film-stack thickness, but is still much smaller than the substrate thickness, G is the same as that of a kink crack from the

pre-crack in a homogeneous elastic material. As mentioned before, the energy release rate of the pre-crack relates to that of the interfacial crack as $G_{\text{pre}} = 3.846G$ [18]. Consequently, the initiation energy relates to the extension energy as

$$\Lambda_{\min} = 3.846\Gamma. \tag{14}$$

For the interfacial crack to extend a distance beyond a few times the film thickness, the energy release rate G_{pre} of the pre-crack must exceed this value. Eq. (14) provides a lower bound to the initiation energy.

This lower bound is attained under two conditions. First, either the pre-existing interfacial flaws are large compared to the film-stack thickness, or the elastic moduli of various materials are similar, so that $G_{\text{pre}} = 3.846G$ is valid. Second, all processes prior to the interfacial crack initiation require an energy release rate G_{pre} lower than 3.846Γ. We next consider scenarios that violate either one of the two conditions, leading to higher values of the initiation energy.

Consider an idealized problem first: a pre-crack perpendicularly impinges upon an interface between two semi-infinite elastic materials. The two materials are dissimilar, one stiffer than the other. At the pre-crack tip, the stress field scales as $\sigma_{ij} \sim r^{-\lambda}$ [20]. The exponent λ depends on the elastic mismatch. Now let the pre-crack deflect onto the interface. The length of the interfacial flaw, a, is the only length in the problem. A dimensional consideration shows that the energy release rate of the interfacial crack scales as $G \sim a^{1-2\lambda}$ [18]. When the pre-crack impinges upon the interface from the more compliant material, $\lambda < 1/2$ and $G \to 0$. When the pre-crack impinges upon the interface from the stiffer material, $\lambda > 1/2$ and $G \to \infty$.

The above problem is the limiting case that the interfacial flaw size is small compared to the film thickness. Next consider the two silicon substrates sandwich a thin elastic film of thickness h, Young's modulus E_{f} and Poisson's ratio ν_{f} (Fig. 12). We further assume that the film has a lower elastic modulus than silicon. We will focus on the situation that the pre-crack emanates from the notch root in the top substrate, penetrates the film, and arrests at the interface between the film and the bottom substrate. On this interface the pre-crack then initiates a new crack. (Appendix A treats the case that the pre-crack stops at the interface between the top substrate and the film.) The above considerations provide the behavior at the two limits, $a/h \to \infty$ and $a/h \to 0$. We fit the energy release rate for the interfacial crack to the following form:

$$G = 0.26\left(1 - \left(1 - \xi_2 (a/h)^{1-2\lambda}\right) \exp(-\xi_1 a/h)\right) G_{\text{pre}}. \tag{15}$$

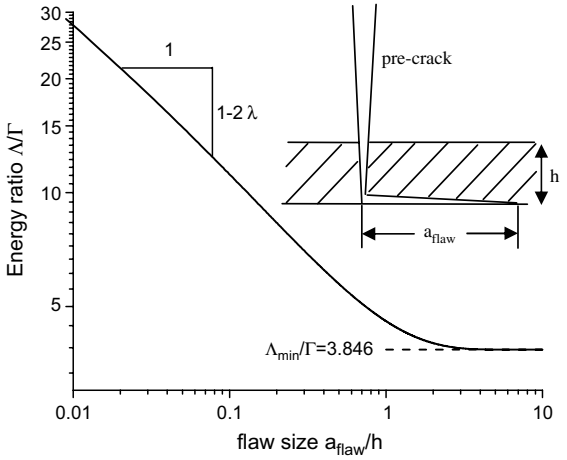

Fig. 12. Initiation-to-extension energy ratio as a function of the flaw size. The film is more compliant than the substrates. The crack propagates on the lower interface.

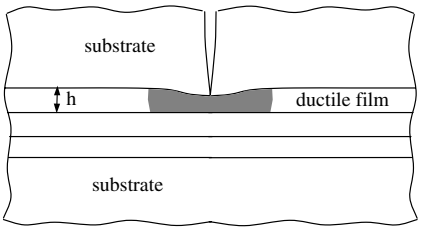

Fig. 13. The pre-crack first ruptures a ductile layer before initiates an interfacial crack.

As a numerical example, $E_f = 10$ GPa and $\nu_f = 1/3$. Our numerical results give $\lambda = 0.333$, $\xi_1 = 0.90$, $\xi_2 = 0.61$. Fig. 12 plots $\Lambda/\Gamma = G_{pre}/G$ as a function of the initial flaw size. As expected, when the initial flaw size a is smaller than the film thickness h, the initiation energy increases. When the flaw size exceeds the film thickness, the result approaches the asymptotes, Eq. (14). When the flaw size is smaller than the film thickness, Λ/Γ is sensitive to the flaw size. This flaw-sensitivity may contribute to the large scatter in the initiation energy observed in the experiments.

Finally we consider the case that the pre-crack needs to rupture a tough film before an interfacial crack initiates (Fig. 13). The load needed to rupture the tough film is higher than that needed to extend the interfacial crack, so that the critical load is associated with rupturing the tough film. Let σ_Y be the yield strength and h be the thickness of the ductile film. According to a well known result in fracture mechanics, the energy release rate needed to rupture the layer is the yield strength times the elongation. The latter is on the order of the film thickness. Thus, the initiation energy is estimated by

$$\Lambda \approx \sigma_Y h. \tag{16}$$

Taking $\sigma_Y = 10^8$ Pa and $h = 10^{-6}$ m, we estimate that the initiation energy is $\Lambda = 100$ J/m^2. This agrees with the order of magnitude of the experimental value for the case that the pre-crack needs to rupture an epoxy layer before the interfacial crack initiates. In this scenario, the initiation energy is governed by the properties of the ductile layer, and is unrelated to the interfacial crack extension energy.

6. Discussions and perspectives

This paper has three basic components: (a) the experimental determination of the initiation energy that characterizes the critical condition under which a pre-crack initiates an interfacial crack, (b) the use of the initiation energy to predict the arrest crack length, and (c) microscopic models of the initiation energy. Each component can be significantly amplified. In the above, to limit the scope of the paper, we have made a number of assumptions. This section discusses the resulting limitations, and outlines perspectives for future work.

We have only considered the case that the two bonding substrates are of the same elastic material. When the two substrates are of dissimilar elastic materials, the Zak–Williams singularity [20] characterizes the stress field in the annulus in Fig. 5. Even though the energy release rate is no longer a valid quantity to characterize the initiation condition, the stress field in the annulus still scales with a single parameter, which can be used to characterize the initiation condition. The procedure should be examined in light of the uses of other elastic singularities to characterize failure conditions (e.g. [21–23]).

We have only considered one type of test configuration: the four-point bend. As such, the analysis of the arrest crack length is considerably simplified by the plateau energy release rate. The mechanics developed in this paper, however, is applicable to any test configuration. In particular, Li et al. [24] has presented a general analysis of beam-like test configurations, including the ones without plateau. It would be significant to

study crack initiation and arrest in other test configurations, and their applications in technologies such as electronic packaging.

We have noted that the experimental values of the crack initiation energy have a larger scatter than those of the crack extension energy. This difference is expected. The initiation energy corresponds to a critical event, and its value is sensitive to the behavior of a single flaw; the extension energy corresponds to a process, and its value results from a large number of uncritical events. Because the energy release rate of the pre-crack, G_{pre}, fully captures the input of the test configuration on the scale of the substrates, we expect that the statistical distribution of the initiation energy (DIE) is independent of the test configuration, but is specific to the bonding materials and processes, as well as the shape and size of the flaws on the interfaces. The DIE can be obtained from the experimental values of initiation energies of multiple samples (e.g., Tables 1 and 2). Once obtained, the DIE can be used to predict the statistical distribution of the critical load in other test configurations involving the same bonding materials and processes. The DIE may also serve as an indication of the quality consistency of a given bonding process.

We have assumed that the interfacial crack extension energy Γ is a constant. In reality, Γ may vary for several reasons. First, Γ depends on the relative amount of sliding and opening mode (e.g. [11]). If the mode mix changes as the interfacial crack extends, Γ varies. A second cause is inelastic deformation around the crack tip, which leads to a resistance curve (e.g. [6]). A third cause is that molecules (such as water) in the environment can assist the bond breaking process at the crack tip, so that the crack extension energy increases with the crack velocity (e.g. [8]). All these factors will affect the initiation, extension and arrest of the interfacial crack. For example, when Γ is a function of the crack velocity, the crack length as a function of time can be calculated from initiation to arrest; no longer do we need to invoke the artificial distinction between overload and underload. As another example, it has been pointed out that crack arrest in buckle-delamination is mainly caused by the increase of Γ with the sliding mode [11].

The crack behavior depends on how the actuation displacement is programmed as a function of time. We have assumed that the displacement is programmed to ramp up. If a feedback control is implemented, so that the displacement can ramp down when the machine senses the interfacial crack initiation, then the force drop does not follow the vertical line in Fig. 3. In the limiting case, the crack can grow under the quasi-equilibrium condition, where the energy release rate G is maintained at the interfacial crack extension energy Γ at all crack lengths. Assume that all prior processes leading to the initiation do not activate the interfacial flaw. The crack starts to grow at the initial flaw size a_{flaw}, which is much smaller than the substrate thickness H. Let $G = \Gamma$ in the two expressions, $G = g(a)L^2P^2/(\overline{E}B^2H^3)$ and $G = g\overline{E}H\Delta^2/(c^2L^2)$. We obtain the force as a function of the crack length, $P(a)$, and the displacement as a function of the crack length, $\Delta(a)$, respectively. Fig. 14 sketches the force–displacement curve for quasi-equilibrium crack propagation, using the crack length as a parameter. When $a \ll H$, the compliance changes negligibly, so that the

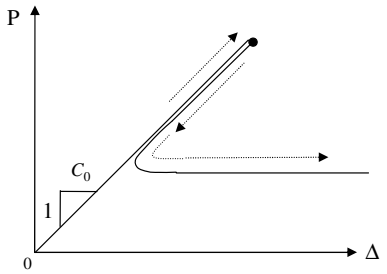

Fig. 14. Schematic of force–displacement curve for quasi-equilibrium crack propagation, where $G = \Gamma$ is maintained at all crack lengths. After the interfacial crack initiates, both the force and displacement decrease. The compliance is nearly constant when the crack length is smaller than the substrate thickness. When the crack length is comparable to the substrate thickness, the force attains a plateau.

force–displacement curve has the constant slope of C_0. As the crack grows, both the force and the displacement decrease, following the essentially the same slope of C_0. When the crack length is comparable to the substrate thickness, the force approaches the plateau, and the displacement increases because the compliance increases with the crack length.

7. Summary

This paper studies an interfacial crack initiated from a pre-crack impinging upon the interface. Upon initiation, the interfacial crack is usually unstable, runs rapidly for a substantial length, and then arrests. We carry out experiments using silicon substrates bonded by thin film stacks, subject to four-point bend. The measured critical force provides a reading of the initiation energy Λ of the interfacial crack. The initiation energy is specific to the film stacks, but is independent of the test configuration on the scale of the substrates. The arrest crack length depends on the crack initiation and extension energy, as well as on the test configuration on the scale of the substrates. The interfacial crack arrests at a short length if the initiation-to-extension energy ratio is small, or the machine compliance is small, or the pre-cracked substrate is thick. The mechanistic models show that the initiation energy has a lower bound that scales with the interfacial crack extension energy, and is sensitive to the interfacial flaws when the flaws are small compared to the film thickness and the elastic modulus of the film is different form that of the substrates. Several lines of future work are outlined.

Acknowledgements

ZYH and ZS acknowledge the financial support of NSF MRSEC, of Intel Corporation, and of the Division of Engineering and Applied Sciences at Harvard University.

Appendix A. Energy release rates for interfacial cracks

The Zak–Williams [20] exponent λ is determined by the equation

$$\cos(\lambda\pi) = \frac{2(\beta-\alpha)}{1+\beta}(1-\lambda)^2 + \frac{\alpha+\beta^2}{1-\beta^2}. \tag{A.1}$$

The Dundurs parameters are

$$\alpha = \frac{\mu_1(\kappa_2+1)-\mu_2(\kappa_1+1)}{\mu_1(\kappa_2+1)+\mu_2(\kappa_1+1)}, \quad \beta = \frac{\mu_1(\kappa_2-1)-\mu_2(\kappa_1-1)}{\mu_1(\kappa_2+1)+\mu_2(\kappa_1+1)}. \tag{A.2}$$

Here $\kappa = 3 - 4\nu$ and $\mu = E/2(1+\nu)$. The subscripts indicate the two materials.

In the body of the text, we give the energy release rate of the interfacial crack in the absence of the thin film, Eq. (12), and that of the interfacial crack between the film and the bottom substrate, Eq. (15). For completeness, we also consider the interfacial crack between the top substrate and the film, with the fitting formula

$$G = \frac{P^2L^2}{\bar{E}H^3B^2}\left[1+\xi_2\left(\frac{a}{h}\right)^{1-2\lambda}\exp\left(-\xi_1\frac{a}{h}\right)\right]\left[1.313-0.313\exp\left(-5.74\frac{a}{H}\right)\right], \tag{A.3}$$

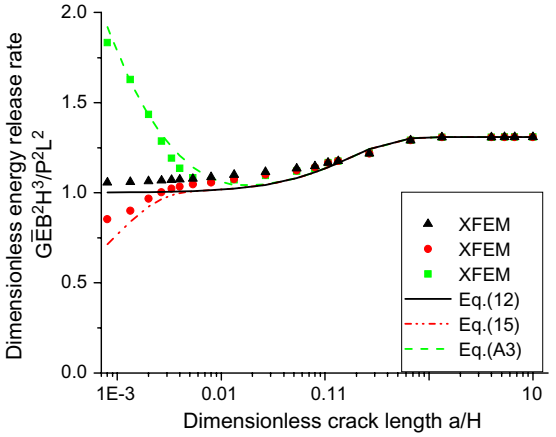

Fig. A.1. A comparison of the computed energy release rate with the fitting formula. This plot assumes that $H/h = 750$.

with $\lambda = 0.8048$, $\xi_1 = 0.234$ and $\xi_2 = 0.78$. In this case, when the interfacial crack length is much smaller than the substrate thickness, the energy release rate decreases as the interfacial crack length increases. Consequently, the initiation energy is given by the lower bound, Eq. (14).

We calculate the energy release rate of the interfacial crack using a general purpose program DYNAFLOW™ [25]. An extended finite element method (XFEM) is implemented for interfacial cracks [26], so that the mesh can be coarse near the crack tip, and the elements need not conform to the crack geometry. Fig. A.1 compares the energy release rate calculated from the finite element method with that of the fitting formulas, Eqs. (12), (15) and (A.3). In all cases, the difference between the finite element results and the fitting formulas is around 5% for very short cracks, and much smaller for long cracks.

References

[1] Hussein MA, He J. Materials impact on interconnects process technology and reliability. IEEE Trans Semicond Manufact, in press.
[2] Suo Z. Reliability of interconnect structures. In: Gerberich W, Yang W, editors. Interfacial and nanoscale failure. Milne I, Ritchie RO, Karihaloo B, editors. Comprehensive structural integrity, vol. 8. Amsterdam: Elsevier; 2003. p. 265–324.
[3] Nix WD. Mechanical-properties of thin-films. Metall Trans 1989;20A:2217–45.
[4] Freund LB, Suresh S. Thin film materials: stress, defect formation and surface evolution. Cambridge: Cambridge University Press; 2003.
[5] Ma Q. A four-point bending technique for studying subcritical crack growth in thin films and at interfaces. J Mater Res 1997;12:840–5.
[6] Lane M. Interface fracture. Annu Rev Mater Res 2003;33:29–54.
[7] Shaffer EO, Mcgarry FJ, Hoang L. Designing reliable polymer coatings. Polym Eng Sci 1996;36:2375–81.
[8] Dauskardt RH, Lane M, Ma Q, Krishna N. Adhesion and debonding of multi-layer thin film structures. Eng Fract Mech 1998;61:141–62.
[9] Hughey MP, Morris DJ, Cook RF, Bozeman SP, Kelly BL, Chakravarty SLN, et al. Four-point bend adhesion measurements of copper and permalloy systems. Eng Fract Mech 2004;71:245–61.
[10] Gerberich WW, Jungk JM, Li Min X, Volinsky AA, Hoehn JW, Yoder K. Int J Fract 2003;119/120:387–405.
[11] Hutchinson JW, Suo Z. Mixed mode cracking in layered materials. Adv Appl Mech 1992;29:63–191.
[12] Evans AG, Hutchinson JW. The thermomechanical integrity of thin films and multilayers. Acta Metall Mater 1995;43:2507–30.
[13] Volinsky AA, Moody NR, Gerberich WW. Interfacial toughness measurements for thin films on substrates. Acta Mater 2002;50:441–66.
[14] Charalambides PG, Lund J, Evans AG, McMeeking RM. A test specimen for determining the fracture resistance of bimaterial interfaces. J Appl Mech 1989;65:77–82.

[15] Cao HC, Evans AG. An experimental study of the fracture resistance of bimaterial interface. Mech Mater 1989;7:295–305.
[16] Lane MW, Liu XH, Shaw TM. Environmental effects on cracking and delamination of dielectric films. IEEE Trans Dev Mater Reliab, in press.
[17] Evans AG. Design and life prediction issues for high-temperature engineering ceramics and their composites. Acta Mater 1997;45:23–40.
[18] He MY, Hutchinson JW. Crack deflection at an interface between dissimilar elastic material. Int J Solids Struct 1989;25:1053–67.
[19] Tada H, Paris PC, Irwin GR. The stress analysis of cracks handbook. St. Louis, MO: Del Research; 1985.
[20] Zak AR, Williams ML. Crack point singularities at a bi-material interface. J Appl Mech 1963;30:142–3.
[21] Liu XH, Suo Z, Ma Q. Split singularities: stress field near the edge of silicon die on polymer substrate. Acta Mater 1999;47:67–76.
[22] Mohammed I, Liechti KM. Cohesive zone modeling of crack nucleation at bimaterial corners. J Mech Phys Solids 2000;48:735–64.
[23] Reedy ED, Guess TR. Comparison of butt tensile-strength data with interface corner stress intensity factor prediction. Int J Solids Struct 1993;30:2929–36.
[24] Li S, Wang J, Thouless MD. The effects of shear on delamination in layered materials. J Mech Phys Solids 2004;52:193–214.
[25] Prévost JH. DYNAFLOW: A nonlinear transient finite element analysis program. Princeton University; 1981 [last updated in 2003].
[26] Sukumar N, Huang ZY, Prévost JH, Suo Z. Partition of unity enrichment for bimaterial interface cracks. Int J Numer Methods Eng 2004;59:1075–102.